

RESEARCH ARTICLE

Effect of bilateral carotid occlusion on cerebral hemodynamics and perivascular innervation: An experimental rat model

M. L. Rots¹  | G. J. de Borst¹ | A. van der Toorn² | F. L. Moll¹ | C. W. A. Pennekamp^{1,3} | R. M. Dijkhuizen² | R. L. A. W. Bleys³

¹Department of Vascular Surgery, University Medical Center Utrecht, Utrecht University, Utrecht, The Netherlands

²Center for Image Sciences, University Medical Center Utrecht, Utrecht University, Utrecht, The Netherlands

³Department of Anatomy, University Medical Center Utrecht, Utrecht University, Utrecht, The Netherlands

Correspondence

R. L. A. W. Bleys, Department of Anatomy, University Medical Center Utrecht, P.O. Box 85060, 3508 AB Utrecht, the Netherlands.
Email: r.l.a.w.bleys@umcutrecht.nl

Abstract

We aimed to investigate the effect of chronic cerebral hypoperfusion on cerebral hemodynamics and perivascular nerve density in a rat model. Bilateral common carotid artery (CCA) ligation ($n = 24$) or sham-operation ($n = 24$) was performed with a 1-week interval. A subgroup (ligated $n = 6$; sham-operated $n = 3$) underwent magnetic resonance imaging (MRI) before the procedures and 2 and 4 weeks after the second procedure. After termination, carotids were harvested for assessment of complete ligation and nerve density in cerebral arteries that were stained for the general neural marker PGP 9.5 and sympathetic marker TH by computerized image analysis. Five rats were excluded because of incomplete ligation. MRI-based tortuosity of the posterior communicating artery (Pcom), first part of the posterior cerebral artery (P1) and basilar artery was observed in the ligated group, as well as an increased volume ($p = 0.05$) and relative signal intensity in the basilar artery ($p = 0.04$; sham-group unchanged). Immunohistochemical analysis revealed that compared to sham-operated rats, ligated rats had increased diameters of all intracircular segments and the extracircular part of the internal carotid artery ($p < 0.05$). Ligated rats showed a higher general nerve density compared to controls in P1 (10%, IQR:8.7–10.5 vs. 6.6%, IQR:5.5–7.4, $p = 0.003$) and Pcom segments (6.4%, IQR:5.8–6.5 vs. 3.2%, IQR:2.4–4.3, $p = 0.003$) and higher sympathetic nerve density in Pcom segments (3.7%, IQR:2.8–4.8 vs. 1.7%, IQR:1.3–2.2, $p = 0.02$). Bilateral CCA occlusion resulted in redistribution of blood flow to posteriorly located cerebral arteries with remarkable changes in morphology and perivascular nerve density, suggesting a functional role for perivascular nerves in cerebral autoregulation.

KEYWORDS

animal model, carotid artery disease, cerebrovascular circulation, innervation, RRID:AB-1143825, RRID:AB-2313713, RRID:AB-92138, RRID:RGD_734476

1 | INTRODUCTION

Cerebral hypoperfusion due to significant steno-occlusive disease has been shown to play an important role in the occurrence of cerebral ischemia (Klijn, Kappelle, Tulleken, & van Gijn, 1997). The hemodynamic effect of a stenosis in the common carotid artery (CCA) on perfusion of the brain tissue depends mainly on the adequacy of collateral circulatory pathways (Powers, 1991; Silesen & Schroeder, 1989). The most important collaterals are formed by the circle of Willis, which connects the internal carotid arteries and the vertebrobasilar system. The functional role of the circle of Willis in serving as a collateral to sustain adequate

cerebral blood flow (CBF) during and after carotid surgery is still unpredictable.

The CBF is dependent on the cerebral perfusion pressure, the diameter of cerebral blood vessels, the viscosity of the blood, as well as factors affecting these parameters (Ursino, 1994). As a result of cerebral autoregulation, CBF is generally unaffected by changes in cerebral perfusion pressure (CPP; difference between the mean arterial pressure and intracranial pressure) provided that CPP is within normal levels (~60–160 mmHg). When CPP is seriously affected and falls outside this range, CBF is directly dependent on CPP (Cipolla, 2009; Silva & Belli, 2018). The exact physiology of these autoregulatory mechanisms has

not yet been clarified but the following mechanisms are thought to interact and contribute to the process of cerebral autoregulation: (a) metabolic or chemical mechanisms: vessel diameter and vascular resistance are affected by the concentration of vasoactive substances involved in tissue metabolism (e.g., O_2 , CO_2 , and H^+), (b) myogenic mechanism: the capacity of vascular smooth muscle to constrict in response to a transmural pressure increase, and (c) neurogenic mechanism: cerebrovascular innervation may be involved in controlling cerebral hemodynamics (Cipolla, 2009). The dense nerve supply to the major cerebral arteries consists of sympathetic, parasympathetic, and sensory fibers (Roloff, Tomiak-Baquero, Kasparov, & Paton, 2016). The regulatory role of sympathetic (vasoconstriction) and parasympathetic (vasodilation) nerve fibers manifests itself by a topographical heterogeneity of nerve densities, corresponding to the potential fluctuations in flow to the concerning brain segment. Perivascular sympathetic innervation has also been demonstrated to induce hypoperfusion after global cerebral ischemia, whereas parasympathetic innervation may play a role in cerebral protection under ischemic circumstances (Lee et al., 2017; Roloff et al., 2016). Importantly, the nerve density has been shown to be dynamic with the capacity to adapt to altering functional demands (Bleys & Cowen, 2001). For example, a decreased metabolic activity induced by anosmia resulted in a decreased overall nerve density in the anterior cerebral artery, the main arterial supplier of the rhinencephalon (Van Denderen, Van Wieringen, Hillen, & Bleys, 2001). Furthermore, a reduction in CBF occurs in both rats and humans due to aging and Alzheimer's disease, respectively, and has been correlated to a decline in overall and sympathetic nerve density in the anterior cerebral artery (Bleys, Cowen, Groen, & Hillen, 1996b; Martin, Friston, Colebatch, & Frackowiak, 1991).

Based on the observation of adapting periarterial nerve density, we hypothesized that permanent bilateral CCA occlusion in rats, will result in local hemodynamic changes and subsequently induce alterations in cerebral artery nerve density. Therefore, the purpose of this study was to evaluate the effects of a staged bilateral CCA occlusion, using an established animal model to study the effect of chronic cerebral hypoperfusion-related changes, on cerebral hemodynamics and nerve density of the basal cerebral arteries in rats (Farkas, Luiten, & Bari, 2007).

2 | MATERIALS AND METHODS

2.1 | Rat ligation model

All animal procedures were carried out under protocols approved by the Animal Experiments Committee of the University Medical Center Utrecht and Utrecht University and in accordance with the guidelines of the European Communities Council Directive.

Forty-eight Crl:CD (Sprague Dawley) rats weighing 300–350 g (Charles River Laboratories, Wilmington, MA, RRID:RGD_734476) were included in the study. Rats were randomly assigned to either bilateral CCA ligation procedure with 1-week interval between the first and the second CCA occlusion (Cechetti, Worm, Pereira, Siqueira, & Netto, 2010) or sham operation (Figure 1).

Both the sham-operated and ligated animals were sacrificed and processed for immunohistochemical studies at 28 days after the second surgical procedure (Van Denderen et al., 2001). All procedures were performed between October 2012 and February 2013 in the morning in the operating rooms of the Central Laboratory Animal Research Facility Utrecht. For ligation or sham-operation animals were premedicated with buprenorphine (0.05 mg/kg i.m.), anesthetized by mechanical ventilation with 4% isoflurane in air (induction) and 2% isoflurane (maintenance). Blood oxygen saturation was continuously monitored during surgical procedures. After shaving and disinfection of the ventral surface of the neck with iodine rats were placed on a heating pad. Rats were randomly assigned to first left-sided or first right-sided operation. Under an operation microscope, a midline ventral incision of 6 cm was made with blade no. 15 and the unilateral carotid artery was bluntly separated from the cervical sympathetic trunk and the vagus nerve. The CCA was subsequently ligated with a 6-0 silk suture. In the 24 sham-operated rats, the CCA was only exposed, but not ligated. After hemostasis intracutaneous wound closure with Vicryl 4-0 was performed. One week after one-sided operation, the contralateral CCA was operated using the primary incision and access route, resulting in 24 rats with bilateral ligation and 24 rats with a bilateral sham procedure.

All procedures were performed after an acclimatization period of 2 weeks. All animals were group-housed under standard, controlled conditions (food and water provided ad libitum, room temperature 22–24°C, 12 hr light/12 hr dark cycle). An entry control with weighing and controls was performed by an animal keeper. Postoperatively, welfare and weight were assessed daily during the first 2 days and weekly during the remaining study period.

2.2 | Magnetic resonance imaging

Magnetic resonance (MR) imaging of the brain in a 4.7T animal MR system (Agilent, Palo Alto, CA) in the first consecutive nine rats (MR-group: ligated $n = 6$ and sham-operated $n = 3$) was performed to evaluate the effect of bilateral ligation on cerebral hemodynamics at three timepoints: $t = 0$ (before ligation), $t = 1$ (2 weeks after bilateral ligation) and $t = 2$ (4 weeks after bilateral ligation, just before sacrifice; see Figure 1). Anesthesia was induced with 4% isoflurane in air followed by administration of 5 ml NaCl 0.9% subcutaneously. During MR scanning, the rats were mechanically ventilated with 2% isoflurane in air. The animals were restrained in the scanner with earplugs and a tooth-holder.



FIGURE 1 Timeline. $t = 0$: preoperative, $t = 1$: 2 weeks after bilateral ligation, and $t = 2$: 4 weeks after bilateral ligation

Body temperature was measured with a rectal probe and was kept at 37°C with a heating pad during the imaging procedure. A home-built Helmholtz volume coil (i.d. 90 mm) was used for signal excitation and a 35 mm inductively coupled surface coil was used for signal reception.

To evaluate whether either changes in volume or relative signal intensity of the basilar artery occurred, two flow-compensated three-dimensional time-of-flight MR angiograms (MRA) of the basal cerebral arteries were acquired (repetition time (TR)/echo time (TE) 20/2 ms, flip angle 40°, field-of-view (FOV) 20 x 25.2 x 15.2 mm³, data matrix size 100 x 126 x 76 points, 4 averages). The second angiogram was acquired 7.5 mm posterior to the first one. Additionally, to determine whether the bilateral occlusion caused a reduced perfusion of the brain, magnetic resonance imaging (MRI) with arterial spin labeling was performed using Flow-Sensitive Alternating Inversion Recovery (Gunther, Bock, & Schad, 2001; Kober, Duhamel, & Cozzone, 2008) combined with a 2-shot gradient-echo EPI acquisition for image read-out (TR/TE 10,000/4.8 ms, delay between images in the inversion curve 150 ms, flip angle 10°, FOV 32 x 32 mm², data matrix 64 x 64, slice thickness 2 mm, selective inversion slab: 10 mm, 16 averages).

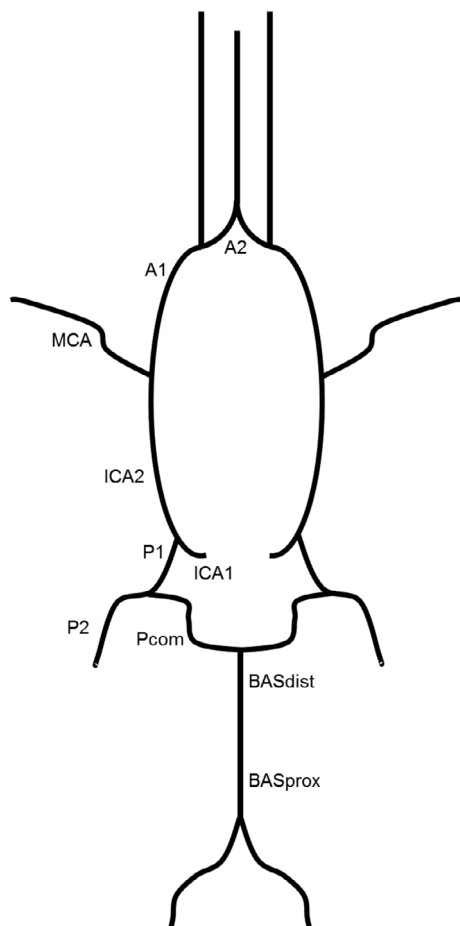


FIGURE 2 Schematic overview of the segments of the circle of Willis. A1: first part of the anterior cerebral artery, A2: second part of the anterior cerebral artery, ICA1: first part of the internal carotid artery, ICA2: second part of the internal carotid artery, MCA: middle cerebral artery, P1: first part of the posterior cerebral artery, P2: second part of the posterior cerebral artery, Pcom: posterior communicating artery, BASprox: proximal part of the basilar artery and BASdist: distal part of the basilar artery

Blood oxygenation level-dependent (BOLD)-MRI with carbogen (5% CO₂, 95% O₂) inhalation as a hypercapnic stimulus was acquired to assess cerebrovascular reactivity. The BOLD acquisition protocol consisted of a two-dimensional single shot spin-echo EPI acquisition (TR/TE 2,000/27 ms, FOV 32 x 32 mm², data matrix size 64 x 64 points, 24 coronal slices of 0.5 mm thickness) repeated 600 times. During the first 150 acquisitions, the rat was ventilated with an air:O₂ (2:1) mixture, followed by 150 acquisitions with 100% O₂. The third set of 150 acquisitions was performed during ventilation with carbogen, and this was followed by 150 acquisitions during ventilation with the air:O₂ mixture again.

2.3 | Tissue preparation

Four weeks after the second operation, the rats were terminated by perfusion fixation with a Watson Marlow SCI 323 peristaltic pump (Watson-Marlow Pumps Group, Falmouth, Cornwall, UK). Under anesthesia (sodium pentobarbital 0.1 ml/100 g body weight i.p.) the ascending aorta was cannulated and the rats were perfused with 300 ml 0.9% NaCl containing 5,000 IE heparin, 500 ml 4% paraformaldehyde in 0.1 M phosphate buffer (pH 7.4, at 4°C), and 500 ml 15% sucrose in 0.1 M phosphate buffer (pH 7.4, at 4°C; Van Denderen et al., 2001). Subsequently, the brains including basal cerebral arteries were removed and stored in 15% sucrose in 0.1 M phosphate buffer (pH 7.4, at 4°C).

2.4 | Immunohistochemistry

After termination, all subjects were macroscopically evaluated for successful carotid ligation. If the ligation was questionable based on both in vivo MRA and postmortem macroscopical evaluation (MR-group) or on postmortem macroscopical evaluation only (non-MR group) these rats were excluded from further analysis. The basal cerebral arteries were dissected of the brain, divided in segments (Figure 2) and mounted on Sylgard (Dow Corning, Midland, MI) with entomology needles. Subsequently, the ligated group ($n = 24$) and sham-operated group ($n = 24$) were divided into three subgroups (each $n = 8$), which underwent various immunohistochemical procedures to localize the general neural marker protein gene product 9.5 (PGP 9.5; ligated $n = 8$ and sham-operated $n = 8$), the parasympathetic nerves containing vesicular acetylcholine transporter (VAcHT; ligated $n = 8$ and sham-operated $n = 8$), or the sympathetic nerves containing tyrosine hydroxylase (TH; ligated $n = 8$ and sham-operated $n = 8$).

The segments that underwent PGP 9.5 staining were washed three times in HEPES buffer containing 0.1% Triton X-100 for 10 min followed by incubation of 5% normal swine serum (Jackson immunoresearch, West Grove, PA) in HEPES buffer containing 0.1% Triton X-100 for 90 min. Subsequently, they were incubated in Rabbit anti-PGP 9.5 (Millipore Cat# AB5925, RRID:AB-92138) diluted 1:400 in HEPES buffer containing 0.1% Triton X-100, 0.1% DL lysine and 1% normal swine serum for 48 hr at 4°C. After 2 days, the segments were washed three times in PBS for 10 min and the segments were incubated in fluorescein isothiocyanate (FITC)-conjugated swine anti-Rabbit serum (Dako, Denmark) diluted in 1:40 in PBS containing 1% normal swine serum, 0.1% Triton X-100, and 0.1% DL-lysine for

90 min. Thereafter, the segments were washed three times in PBS for 10 min and stained for 10 min in 0.05% pontamine sky blue (Gurr, Poole, UK) to reduce background autofluorescence and washed in PBS three times for 5 min (Cowen, Haven, & Burnstock, 1985). Lastly, the segments were stretched on glass slides and mounted with Vectashield (Vector Laboratories, Inc., Burlingame, CA) mounting medium.

Segments that underwent VACHT staining were washed three times in Hepes buffer containing 0.1% Triton X-100 for 10 min followed by incubation of 5% normal goat serum (Jackson immunoresearch, West Grove, PA) in Hepes buffer containing 0.1% Triton X-100 for 90 min. The segments were subsequently incubated overnight at room temperature in Rabbit anti-VACHT (Abcam CAT# ab68984, RRID:AB-1143825) diluted 1:1,500 in Hepes buffer containing 0.1% Triton X-100, 0.1% DL lysine, 1% normal goat serum, and 5% bovine serum albumin (Across Organics, Fair Lawn, NJ) After washing three times in PBS for 10 min, the segments were incubated in Streptavidin FITC (Dako, Denmark) diluted in 1:1,000 in PBS containing 0.1% Triton X-100 and 0.1% DL-lysine for 90 min. Thereafter, the segments were washed three times in PBS for 10 min and stained for 10 min in 0.05% pontamine sky blue and washed in PBS three times for 5 min. Lastly, the segments were stretched on glass slides and mounted with Vectashield mounting medium.

Segments that underwent TH staining were washed three times in Hepes buffer containing 0.1% Triton X-100 for 10 min followed by incubation of 5% normal swine serum (Jackson immunoresearch, West Grove, PA) in Hepes buffer containing 0.1% Triton X-100 for 90 min and subsequently incubated overnight at room temperature in Rabbit anti-TH (Pel-Freez biologicals Cat# P40101, RRID:AB-2313713)

diluted 1:400 in Hepes buffer containing 0.1% Triton X-100, 0.1% DL lysine, and 1% normal swine serum. The next day, the segments were washed three times in PBS for 10 min and incubated in FITC-conjugated swine anti-Rabbit serum diluted in 1:40 in PBS containing 1% normal swine serum, 0.1% Triton X-100, and 0.1% DL-lysine for 90 min. Next, the segments were washed three times in PBS for 10 min and stained for 10 min in 0.05% pontamine sky blue and washed in PBS three times for 5 min. Lastly, the segments were stretched on glass slides and mounted with Vectashield mounting medium.

2.5 | Image processing and analysis

For quantification of PGP 9.5, VACHT and TH immunoreactivity at the adventitial-medial border in the segments of the basal cerebral arteries (Figure 2) microscope slides were reviewed using an Axiophot fluorescence microscope (Carl Zeiss, Oberkochen, Germany) and images were obtained at 20x using a Leica digital camera (DFC 420C, Leica Camera, AG, Germany) and Leica application Suite acquisition software. Images were imported in the public domain software for image analysis, ImageJ, and subjected to an established method of image analysis (Cowen & Thrasivoulou, 1990) Although the observer was blinded to ligation status, the diameters of the basal cerebral arteries were measured and in each image, the area percentage (percentage of specific fluorescence in the measuring frame) was scored in three randomly chosen fields, which were subsequently averaged and used for further analysis.

The two consecutively made MRA images were combined into one image for visual inspection (observer blinded to ligation status) where the anterior part of the posterior image was removed in favor of the anterior image. The images were also normalized to compensate for the signal decay as a result of the use of a surface coil. In each individual MRA image, the area containing the basilar artery was manually selected. The number of voxels with a signal intensity above a threshold of 20% of the maximum signal intensity in the selected area was counted as belonging to the basilar artery. Multiplication with the voxel dimensions thus provides apparent artery volumes.

Apparent CBF values were obtained by manually selecting the brain in the last images of the non-slice-selective inversion series. The signal intensity of this region of interest was summed for each image in each inversion series. The signal difference between the signal intensity of the non-slice-selective inversion series was subtracted from the slice-selective image series. Fitting of the signal difference curve to a modified equation has been previously described by Gunther et al. (2001) and Kober et al. (2008). Time-dependent signal intensities as a result of the BOLD effect during a carbogen challenge were obtained by manually outlining the rat's brain in the images and averaging the signal intensity of all voxels in the brain. This signal was normalized by dividing it with the mean signal intensity obtained during the air/O₂ ventilation period at the start. Changes in signal intensity were observed relative to this signal intensity.

2.6 | Sample size calculation and statistical analysis

This study had a statistical power of 90% to identify a difference of 3.0 area-percent nerve density, given a two-sided α value of 0.05 and a standard deviation of 1.7 (Van Denderen et al., 2001). Sample size

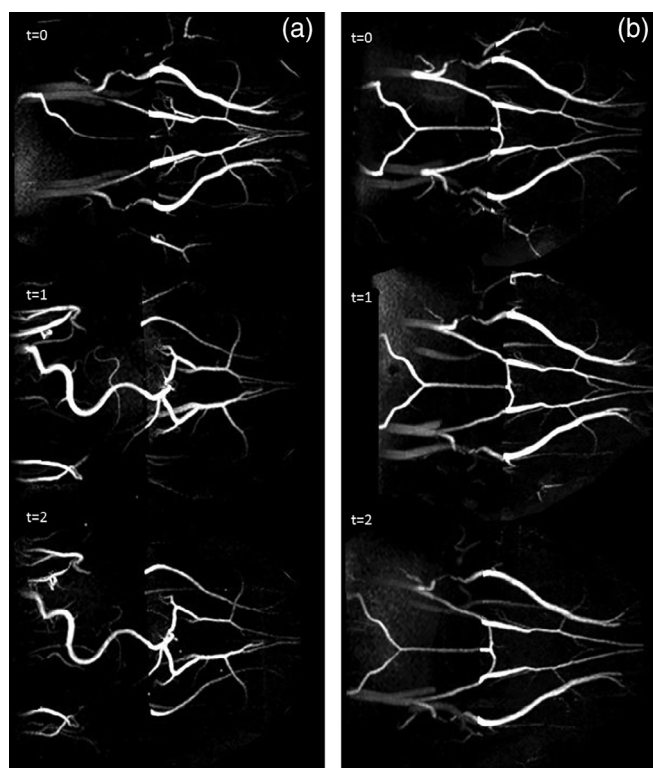


FIGURE 3 MR images of the three animals of the ligated (a) and sham-operated (b) group at $t = 0$ (preoperative), $t = 1$ (2 weeks after bilateral ligation) and $t = 2$ (4 weeks after bilateral ligation)

calculation for detection of the difference between ligated and sham-operated rats, resulted in the need of eight rats in each of the six subgroups (PGP 9.5, VAcHT and TH staining in ligated as well as in control rats); a total of 48 rats were required. Continuous variables are presented as median (IQR: interquartile range). Due to the limited sample size, nonparametric tests were used. Nerve densities between groups were compared using the Mann–Whitney *U* test, whereas the Friedman test was used for comparison of multiple groups with repeated measures. All analyses were performed using commercially available statistical software (SPSS 20.0, SPSS Inc., Chicago, IL). A two-sided *p* value <0.05 was considered significant.

3 | RESULTS

3.1 | Ligation procedure and macroscopical analysis

All rats survived the whole study period. Two rats developed a subcutaneous hematoma following surgery, which was relieved during the second procedure. In six rats, unilateral ptosis was observed postoperatively, which persisted till termination. Based on in vivo MRA uncertainty on the achieved occlusion existed in two rats (MR-group). Postmortem macroscopical evaluation revealed unsuccessful ligation in these and in three other (non-MR group) rats. Subsequently, these five rats were excluded for further analysis, according to the protocol. In the sham-operated rats, the CCAs were patent at *t* = 0, *t* = 1, and *t* = 2.

3.2 | Magnetic resonance imaging

In all ligated rats, an increase in tortuosity of the posterior communicating artery (Pcom segment) and first part of the posterior cerebral artery (P1 segment) and the basilar artery was observed at *t* = 1 and *t* = 2, compared to *t* = 0; see Figure 3. In the ligated rats, a significantly increased median volume of the basilar artery (*p* = 0.05) and relative signal intensity in the basilar artery (*p* = 0.04) were measured (Table 1a). In the sham-operated rats, no tortuosity of the basilar artery was observed at *t* = 0, *t* = 1, and *t* = 2. Median volumes and relative median signal intensity of the basilar artery remained unchanged (both *p* = 0.72).

3.3 | Carbogen challenge

In all rats, an increase in signal intensity was observed at *t* = 0, *t* = 1, and *t* = 2 for both the switch from air to oxygen and for the switch from oxygen to carbogen, without significant difference between sham-operated and ligated rats.

3.4 | Perfusion measurements

No significant differences in apparent CBF between the ligated and sham-operated rats were found (Table 1b). The observed differences fell within the natural range of deviations.

3.5 | Immunohistochemistry analysis

As shown in Table 2, the diameters of the first part of the anterior cerebral artery (A1; median 1.00 mm, IQR: 0.88–1.08, vs. median 0.82 mm, IQR: 0.77–0.93, *p* = 0.03), first part of the carotid artery (ICA1; median 1.21 mm, IQR: 1.09–1.27 vs. median 1.06 mm, IQR: 1.00–1.17, *p* = 0.03), second part of the carotid artery (ICA2; median 1.15 mm, IQR: 1.02–1.24 vs. median 0.98 mm, IQR: 0.88–1.12, *p* = 0.02), P1 segment (median 0.99 mm, IQR: 0.82–1.14 vs. median 0.83 mm, IQR: 0.78–0.89, *p* = 0.05) and Pcom segment (median 0.99 mm, IQR: 0.82–1.14 vs. median 0.65 mm, IQR: 0.48–0.69, *p* < 0.001) in the ligated rats were significantly larger compared to diameters in the sham-operated rats.

3.6 | PGP 9.5 immunoreactivity

In all studied segments, PGP 9.5 immunoreactivity was seen in the deep nerve plexus at the adventitial medial border. The PGP 9.5 nerve density was greatest in the anterior segments of the basal cerebral arteries (Table 3a, Figure 4). The ligated animals compared to the sham-operated animals had a significantly higher nerve density, in both the P1 segment, median area 10.1% (IQR: 8.7–10.5) versus 6.6% (IQR: 5.5–7.4), *p* = 0.003 and the Pcom segment, median area 6.4% (IQR: 5.8–6.5) versus 3.2% (IQR: 2.4–4.3), *p* = 0.003 (Figure 5). When rats with ptosis were excluded, the nerve density in the P1 segment and Pcom segment were still significantly different between the ligated and sham-operated rats (both *p* = 0.006, data not shown).

TABLE 1 Results of MRI volume and perfusion measurements of ligated and sham-operated rats

a.					
Basilar artery volumes (μl)		t = 0	t = 1	t = 2	p Value
Ligated	Median (IQR)	16 (14–18)	29 (26–47)	34 (25–42)	0.05*
Sham	Median (IQR)	20 (19–21)	22(18–29)	21 (18–28)	0.72
Relative signal intensity (%)					
Ligated	Median (IQR)	0.0031 (0.0018–0.0045)	0.011 (0.0097–0.0122)	0.0095 (0.0074–0.0107)	0.04*
Sham	Median (IQR)	0.0040 (0.0036–0.0068)	0.0048 (0.0016–0.0051)	0.0072 (0.0043–0.0079)	0.72
b.					
CBF (ml/100 g)		t = 0	t = 1	t = 2	p Value
Ligated	Median% (IQR)	303 (283–334)	278 (211–287)	268 (218–313)	0.26
Sham	Median% (IQR)	299 (232–580)	312 (236–393)	269 (224–317)	0.37

Median values and interquartile range (IQR) volumes (μl) and relative signal intensity (%) of the basilar artery (a) and apparent cerebral blood flow values (CBF, b: ml/100 g/min) in the ligated and sham-operated rats at *t* = 0 (preoperative), *t* = 1 (2 weeks after bilateral ligation) and *t* = 2 (4 weeks after bilateral ligation). Statistically significant differences are indicated by an asterisk (*).

TABLE 2 Diameters of investigated artery segments of ligated and sham-operated rats

Diameter (mm)	ICA1	ICA2	MCA	A1	A2	P1	P2	Pcom	Bas
Ligated	Median (IQR) 1.21 (1.09–1.27)	1.15 (1.02–1.24)	0.94 (0.68–1.11)	1.00 (0.87–1.08)	0.99 (0.73–1.07)	0.99 (0.82–1.14)	0.74 (0.58–0.89)	0.99 (0.82–1.14)	0.97 (0.84–1.30)
	N	13	12	14	13	13	15	12	4
Sham	Median (IQR) 1.06 (1.00–1.17)	0.98 (0.88–1.12)	0.75 (0.68–0.82)	0.82 (0.77–0.93)	0.90 (0.75–1.03)	0.83 (0.78–0.89)	0.69 (0.60–0.79)	0.65 (0.48–0.69)	0.95 (0.81–1.04)
	N	20	21	21	17	18	20	16	4
p Value	0.03*	0.02*	0.08	0.03*	0.49	0.05*	0.40	<0.001*	0.56

Median diameters (mm) and interquartile range (IQR) in various segments of the basal cerebral arteries from ligated and sham-operated animals. ICA1: first part of the internal carotid artery; ICA2: second part of the internal carotid artery; MCA: middle cerebral artery; A1: first part of the anterior cerebral artery; A2: second part of the anterior cerebral artery; P1: first part of the posterior cerebral artery; P2: second part of the posterior cerebral artery; Pcom: posterior communicating artery; BAS: basilar artery. Statistically significant values are indicated by an asterisk (*).

3.7 | VACHt immunoreactivity

VACHt staining generally resulted in unsatisfactory color contrast, making it impossible to perform computerized image analysis of VACHt reactivity (Figure 4). Visual impression of the presence of VACHt containing nerves revealed that VACHt was present in the circular oriented terminal plexus at the adventitial medial border in all investigated segments.

3.8 | TH immunoreactivity

In all studied segments, TH immunoreactivity was observed in the deep nerve plexus at the adventitial medial border (Table 3b, Figure 4). The topographical distribution did not differ between the ligated and sham-operated group. The highest sympathetic nerve density was found in the anterior segment of the circle of Willis. Nerve density in the Pcom segment was significantly higher in the ligated group than the sham-operated group, median 3.7% (IQR: 2.8–4.8) versus 1.7% (IQR: 1.3–2.2, $p = 0.02$; Figure 5). When rats with ptosis were excluded, the difference remained significant ($p = 0.02$, data not shown).

4 | DISCUSSION

The major findings of this study are the remarkable changes in morphology and nerve density of the posteriorly located basal cerebral arteries that developed after bilateral CCA ligation in rats. The procedure induced a major redistribution of blood supply to the head accompanied by increased flow fluctuations through the vertebral and basilar arteries, resulting in increased basilar artery and Pcom tortuosity, enlargement of several segments and concurrent increase in the nerve supply of the Pcom and P1 segments. However, in the applied animal model, no significant changes in cerebral perfusion or cerebrovascular reactivity were measured during MRI follow-up. These findings suggest that the brain's undiseased vascular system has a large adaptation range to compensate the bilateral CCA ligation.

4.1 | Changes in cerebral arterial morphology and hemodynamics

Previously, bilateral CCA occlusion in rodents has been performed to study the effects of chronic hypoperfusion on cognitive dysfunction, neurogenerative processes, ischemic white matter injury, and ischemic eye disease (Farkas et al., 2007). The fact that bilateral CCA occlusion did not result in significant chronic cerebral hypoperfusion in the current study may be explained by the surgical procedure. In our experience (unpublished data), confirmed by others (Cechetti et al., 2010), contemporaneously bilateral CCA ligation in rats was followed by progressive neurologic deterioration in the first 48 hr postoperatively with a survival rate of <10–40%. Therefore, we used a modified surgical procedure with a 1-week interval between the ipsilateral and contralateral ligation to avoid a too abrupt reduction of CBF, resulting in a 100% survival rate (Tsuchiya, Sako, Yura, & Yonemasu, 1992). It has been shown previously that gradual occlusion of a vessel results in a less deleterious effect on the tissue elements of the distal territory in comparison to an abrupt occlusion (Kaliszewski, Fernandez, & Wicke, 1988), while changes in cognitive impairment are comparable to the conventional model.

TABLE 3 Nerve densities of investigated artery segments of ligated and sham-operated rats

a.												
	ICA1	ICA2	MCA	A1	A2	P1	P2	P-com	Bas-prox	Bas-dist		
Sham	Median% (IQR)	20.3 (19.1–23.1)	10.6 (9.5–11.5)	28.9 (24.3–29.3)	27.4 (23.3–29.4)	6.6 (5.4–7.4)	5.6 (4.7–6.3)	3.2 (2.4–4.3)	3.7 (3.1–7.6)	3.9 (3.5–5.6)		
	N	10	10	10	8	8	10	8	5	7		
Ligated	Median% (IQR)	18.9 (17.8–21.4)	8.8 (5.4–10.5)	24.3 (23.5–25.6)	25.9 (21.3–27.1)	10.1 (8.7–10.5)	6.3 (5.2–7.9)	6.4 (5.8–6.5)	8.5 (4.1–12.5)	5.7 (4.3–6.5)		
	N	5	5	6	5	6	7	5	3	4		
	p Value	0.27	0.11	0.08	0.38	0.003*	0.08	0.003*	0.18	0.09		
b.												
	ICA1	ICA2	MCA	A1	A2	P1	P2	P-com	Bas-prox	Bas-dist		
Sham	Median% (IQR)	16.6 (15.3–19.8)	14.7 (12.3–16.3)	23.8 (19.0–29.0)	20.7 (15.7–28.0)	4.9 (3.7–7.6)	3.9 (3.7–5.0)	1.7 (1.3–2.2)	4.7 (2.7–6.9)	3.9 (3.2–4.3)		
	N	10	10	10	8	9	10	6	10	7		
Ligated	Median% (IQR)	16.3 (13.4–18.3)	14.3 (13.1–17.4)	19.3 (17.4–22.5)	20.9 (18.8–21.8)	4.4 (3.8–7.0)	3.8 (2.8–8.5)	3.7 (2.8–4.8)	6.8 (3.9–8.8)	4.9 (3.3–5.8)		
	N	7	7	8	6	7	7	4	5	5		
	p Value	0.50	0.92	0.05	0.70	0.63	0.85	0.02*	0.22	0.17		

Median values and interquartile range (IQR) area percentage of PGP 9.5-immunoreactive nerve fibers (a) and TH-immunoreactive nerve fibers (b) in various segments of the basal cerebral arteries from sham-operated and ligated animals. ICA1: first part of the internal carotid artery; ICA2: second part of the internal carotid artery; MCA: middle cerebral artery; A1: first part of the anterior cerebral artery; A2: second part of the anterior cerebral artery; P1: first part of the posterior cerebral artery; P2: second part of the posterior cerebral artery; P-com: posterior communicating artery; BAS-prox: proximal part of the basilar artery; and BAS-dist: distal part of the basilar artery. N = number of rats. Statistically significant values are indicated by an asterisk (*).

Possibly, CBF was reduced immediately after ligation of the second CCA, but normalized when measured by MRI 2 weeks after surgery, which is in agreement with a similar rabbit model suggesting adaptation to normal perfusion within 5 days (Tutino et al., 2014). Chronic CBF recovery after bilateral CCA ligation in rats has been observed previously, however, CBF remained slightly but significantly decreased up to at least 4 weeks after bilateral CCA ligation as compared to controls (Otori et al., 2003). An increase of vascular diameter was observed in all intracircular segments of the basal cerebral arteries and in ICA1. This was expected for the vessels that connect the basilar and the internal carotid arteries, Pcom and P1, of which the PCom, connecting the posterior and anterior parts of the circle, showed the highest increase (52%). Apparently, flow redistribution following the bilateral carotid ligation all anastomosing segments of the circle of Willis have to adapt to ensure sufficient cerebral perfusion. Dilatation of the afferent ICA1 (distal to the ligation), secondary to retrograde supply to external carotid branches, may reflect its inability to release its contents. Interestingly, the basilar artery did not show an increase in diameter during microscopical analysis but showed elongation and tortuosity during in vivo MR only. The diameters of all efferent arteries, A2, MCA, and P2, did not change in agreement with a normal cerebral perfusion.

As reported in a previous study, we observed that the cerebrovascular reactivity was not affected 2 weeks following bilateral CCA ligation. This suggests that vasodilatation is not the primary mechanism for CBF maintenance or recovery (Choy et al., 2006).

4.2 | Changes in perivascular nerve density

The current observation that nerve density in the posteriorly located basal cerebral arteries increases with a rise in blood flow, is in line with previous findings that the regional nerve density correlates with local blood flow (Choy et al., 2006) and has the capacity to adapt to altering functional demands (Bleys & Cowen, 2001). Moreover, perivascular sympathetic nerves are capable of effectuating alterations in cerebral perfusion (Edvinsson & Hamel, 2002; Sercombe et al., 1975) and elimination of sympathetic innervation has been shown to protect from cerebral hypoperfusion under ischemic conditions (Lee et al., 2017). It seems that changes in flow and pressure trigger the cerebrovascular innervation to adapt until a new optimal innervation pattern is reached. We hypothesize that neurotrophic factors are released in response to local changes in flow and pressure, resulting in an increase in sympathetic nerve density to keep CBF within normal range. Our findings support the hypothesis that the sympathetic nerves play a functional role in regulation of CBF and are therefore part of the autoregulation mechanism. Considering the observed patterns of altered diameters and nerve densities, we suggest that the hemodynamic changes that occurred had to reach a threshold to trigger these morphological changes.

4.3 | Limitations

Because of restrictions in the number of subgroups and number of animals to be used in this study, we chose to terminate all rats after 4 weeks, which was considered to be the most likely period to detect permanent changes based on a prior study (Van Denderen et al., 2001). It is unclear whether the changes in nerve density as observed in the current study are

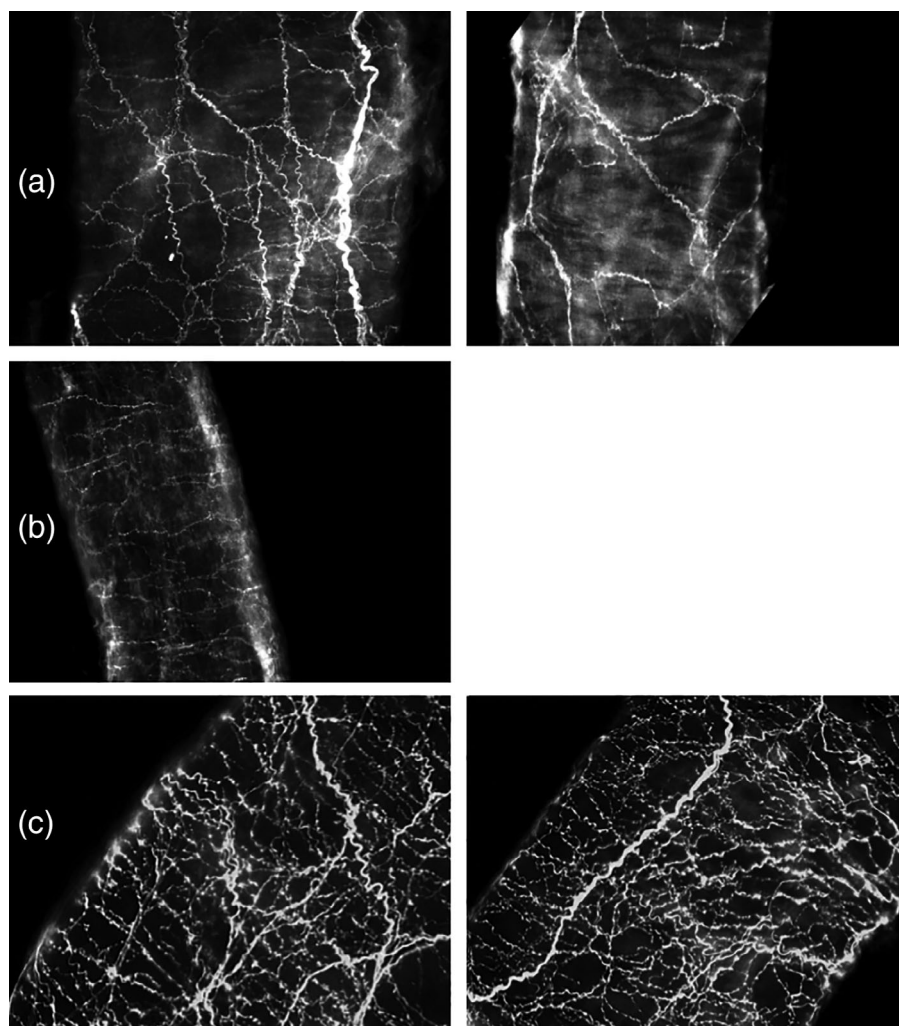


FIGURE 4 (a) Whole mount preparations of perivascular nerves stained for PGP 9.5, Pcom segment of a ligated (left) and a sham-operated rat (right). (b) Whole mount preparations of perivascular nerves stained for vesicular acetylcholine transporter, P1 segment of a ligated rat. (c) Whole mount preparations of perivascular nerves stained for TH, A1 segment of a ligated (left), and sham-operated (right) rat (not significant). For abbreviations, see Table 2 legend

temporary or permanent. It may be interesting to study whether these changes are reversible and disappear after restoration of blood flow in the carotid artery. From the clinical point of view, it would be of importance to understand autoregulatory mechanisms after operating the contralateral carotid artery in case of ipsilateral carotid occlusion for the need for intraoperative shunting, as well as the risk for postoperative hyperperfusion. Nonetheless, we are presently unaware on the clinical significance of the found differences in nerve densities. We ligated the CCA and not solely the ICA. Therefore, the entire cranial circulation was affected instead of only the intracranial part. The reason for this approach was the close topographical relationship of the ICA and the superior cervical ganglion and as a consequence a potential disruption of the sympathetic innervation of the cerebral arteries when performing a ligation of the ICA.

The used MR methods can be discussed. The TOF method is dependent on the arterial flow and flow velocity. The initial flow through the rat's basilar artery may have been too low for robust visualization using MRA with the chosen settings. After bilateral CCA occlusion, the flow presumably increases which improves the reliability of detection of the basilar artery. Consequently, the measurements of the volume of the vessel in MRA should be interpreted with caution and data were used to

further support our findings of increased diameters in the ligated group. As these changes did not occur in the sham-operated group, we believe that these changes are most likely due to the ligation procedure.

In six rats ptosis was observed, however, as no significant difference between rats with and without ptosis was found, we do not believe the ptosis was a symptom of a complete interruption of the sympathetic nervous system and we did not exclude these rats from our analysis. VACHT staining resulted in poor color contrast, making it impossible to perform computerized image analysis. This may be due to the localization of the antigen. VACHT is involved in transporting acetylcholine into synaptic vesicles and, therefore, it is mainly present in neuron cell bodies, where it is synthesized, and in nerve terminals. In the autonomic nervous system, transmitters are released from varicosities that are distributed over the terminal nerve plexuses. As a result, the staining shows many small spots, which do not always allow for computerized image analysis.

4.4 | Translation to humans

Animal studies are required to gain more insight on the influence of redistribution of blood flow on cerebrovascular innervation. Moreover,

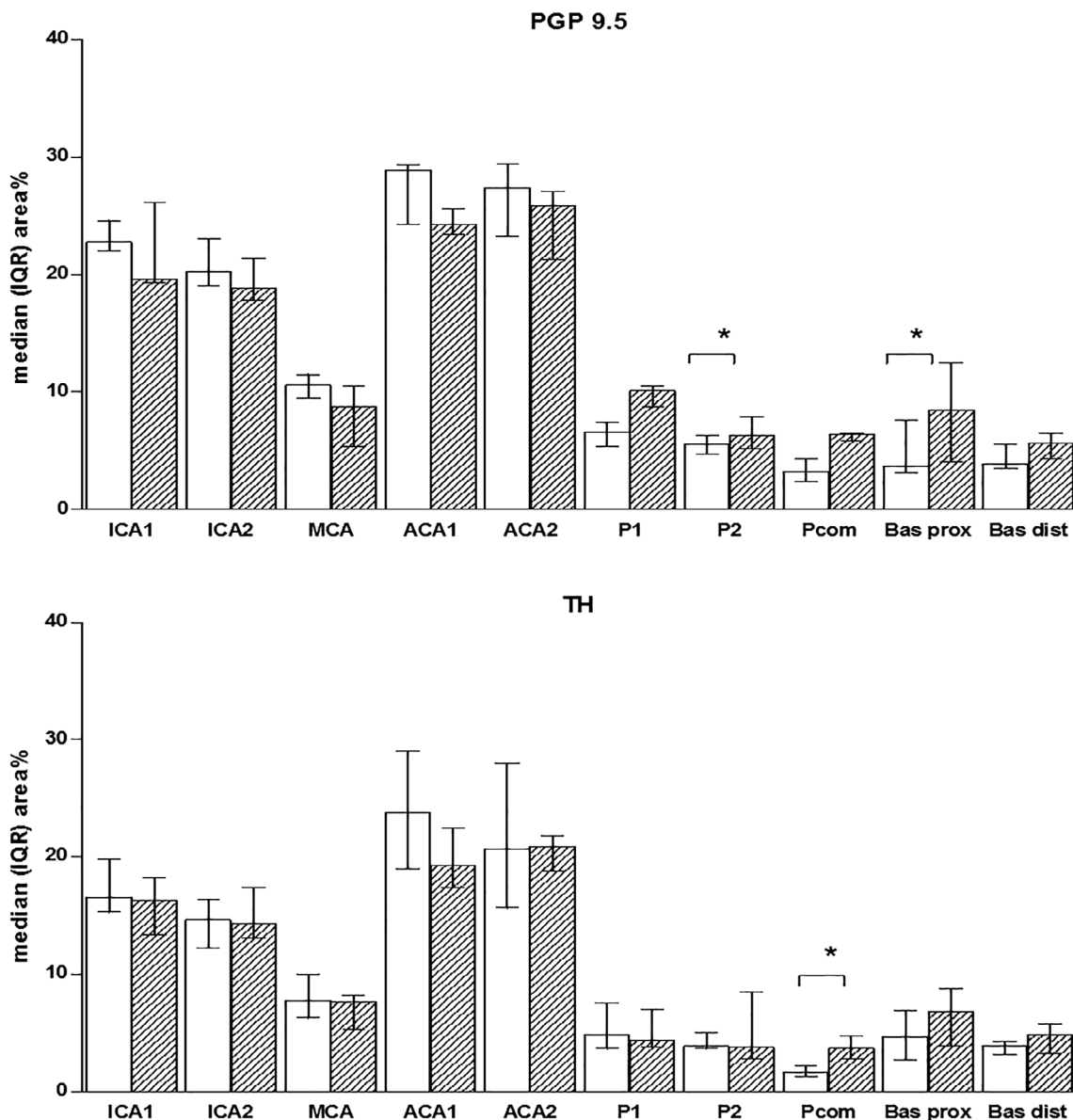


FIGURE 5 Median values and interquartile range (IQR) area percentage of PGP 9.5-immunoreactive nerve fibers (a) and TH-immunoreactive nerve fibers (b) in various segments of the basal cerebral arteries from sham-operated (white) and ligated animals (striped). For abbreviations, see Figure 2 legend. Statistically significant values are indicated by an asterisk (*)

in experimental animal studies, influence of several other factors such as degenerative processes, aging, silent cerebral embolism, and diabetes mellitus can be excluded (Sercombe et al., 1975). A different topographical distribution of the nerve density in the vascular system between humans and rats does exist. In humans, the posterior segment of the cerebral circulation has been described as most densely innervated, whereas in rats the highest nerve density was found in the anterior cerebral artery (Bleys & Cowen, 2001; Bleys, Cowen, Groen, & Hillen, 1996a). As this contrast might be due to a high metabolic need of the target vascular territory, (i.e., the visual cortex in humans and rhinencephalic structures in rats), we do not believe this difference influenced our results. We acknowledge that in humans, as opposed to healthy rats, carotid artery disease is an indicator of generalized atherosclerosis and that intracranial carotid artery disease often coexists (Kappelle, Eliasziw, Fox, Sharpe, & Barnett, 1999). In addition, progressive generalized atherosclerosis

may limit compensatory mechanisms in man, ultimately resulting in watershed infarction.

4.5 | Conclusion

Our findings in the rat model provide support for the hypothesis that bilateral CCA occlusion results in alterations in cerebral hemodynamics and nerve density and underline close morphological and functional relationships of working mechanisms in the basal cerebral arteries.

ACKNOWLEDGMENTS

We thank Mr. J. W. de Groot for assistance with immunohistochemistry and Dr. T. A. P. Roeling for technical help with image analysis.

ORCID

M. L. Rots  <https://orcid.org/0000-0002-3751-0376>

REFERENCES

- Bleys, R. L., Cowen, T., Groen, G. J., & Hillen, B. (1996a). Perivascular nerves of the human basal cerebral arteries: I. Topographical distribution. *Journal of Cerebral Blood Flow and Metabolism*, 16, 1048–1057.
- Bleys, R. L., Cowen, T., Groen, G. J., & Hillen, B. (1996b). Perivascular nerves of the human basal cerebral arteries II. Changes in aging and Alzheimer's disease. *Journal of Cerebral Blood Flow and Metabolism*, 16(5), 1048–1057. <https://doi.org/10.1097/00004647-199609000-00030>
- Bleys, R. L. A. W., & Cowen, T. (2001). Innervation of cerebral blood vessels: Morphology, plasticity, age-related, and Alzheimer's disease-related neurodegeneration. *Microscopy Research and Technique*, 53, 106–118.
- Cechetti, F., Worm, P. V., Pereira, L. O., Siqueira, I. R., & Netto, C. A. (2010). The modified 2VO ischemia protocol causes cognitive impairment similar to that induced by the standard method, but with a better survival rate. *Brazilian Journal of Medical and Biological Research*, 43(12), 1178–1183. <https://doi.org/10.1590/S0100-879X2010007500124>
- Choy, M., Ganesan, V., Thomas, D. L., Thornton, J. S., Proctor, E., King, M. D., ... Lythgoe, M. F. (2006). The chronic vascular and haemodynamic response after permanent bilateral common carotid occlusion in newborn and adult rats. *Journal of Cerebral Blood Flow and Metabolism*, 26(8), 1066–1075. <https://doi.org/10.1038/sj.jcbfm.9600259>
- Cipolla, M. J. (2009). Control of cerebral blood flow. In D. N. Granger, & J. Granger (Eds.), *The cerebral circulation*. San Rafael, CA: Morgan & Claypool Life Sciences. Retrieved from <https://www.ncbi.nlm.nih.gov/books/NBK53082/#top>
- Cowen, T., Haven, A. J., & Burnstock, G. (1985). Pontamine sky blue: A counterstain for background autofluorescence in fluorescence and immunofluorescence histochemistry. *Histochemistry*, 82(3), 205–208. <https://doi.org/10.1007/BF00501396>
- Cowen, T., & Thrasivoulou, C. (1990). Cerebrovascular nerves in old rats show reduced accumulation of 5-hydroxytryptamine and loss of nerve fibres. *Brain Research*, 513(2), 237–243. [https://doi.org/10.1016/0006-8993\(90\)90461-J](https://doi.org/10.1016/0006-8993(90)90461-J)
- Edvinsson, L., & Hamel, E. (2002). Perivascular nerves in brain vessels. In L. Edvinsson & D. N. Krause (Eds.), *Cerebral blood flow and metabolism* (pp. 43–67). Philadelphia, PA: Lippincott Williams & Wilkins.
- Farkas, E., Luiten, P. G. M., & Bari, F. (2007). Permanent, bilateral common carotid artery occlusion in the rat: A model for chronic cerebral hypoperfusion-related neurodegenerative diseases. *Brain Research Reviews*, 54(1), 162–180. <https://doi.org/10.1016/j.brainresrev.2007.01.003>
- Gunther, M., Bock, M., & Schad, L. R. (2001). Arterial spin labeling in combination with a look-locker sampling strategy: Inflow turbo-sampling EPI-FAIR (ITS-FAIR). *Magnetic Resonance in Medicine*, 46(5), 974–984. <https://doi.org/10.1002/mrm.1284>
- Kaliszewski, C., Fernandez, L. A., & Wicke, J. D. (1988). Differences in mortality rate between abrupt and progressive carotid ligation in the gerbil: Role of endogenous angiotensin II. *Journal of Cerebral Blood Flow and Metabolism*, 8(2), 149–154. <https://doi.org/10.1038/jcbfm.1988.43>
- Kappelle, L. J., Eliasziw, M., Fox, A. J., Sharpe, B. L., & Barnett, H. J. (1999). Importance of intracranial atherosclerotic disease in patients with symptomatic stenosis of the internal carotid artery. The North American Symptomatic Carotid Endarterectomy Trial. *Stroke*, 30(2), 282–286. Retrieved from [papers://490fc991-209f-415a-8b63-00fb1df9aa5/Paper/p3230](https://pubs.rsos.royalsocietypublishing.org/doi/10.1098/rsos.190100)
- Klijn, C. J. M., Kappelle, L. J., Tulleken, C. A. F., & van Gijn, J. M. (1997). Symptomatic carotid artery occlusion: A reappraisal of hemodynamic factors. *Stroke*, 28(10), 2084–2093. Retrieved from <https://ovidsp.tx.ovid.com/sp-3.31.1b/ovidweb.cgi?QS2=434f4e1a73d37e8c5536fae4e70f46a0737da32dcd772776b47d7f7ae148f62527f592fa7043fcedb448298bbca1c3f82d848f46615c6511cc2efb0da2b2e947f80f2d411487ee83d41be7f3ee09f8c07394e6072f833e181c040e11c4cfc8254f30eb9064>
- Kober, F., Duhamel, G., & Cozzone, P. J. (2008). Experimental comparison of four FAIR arterial spin labeling techniques for quantification of mouse cerebral blood flow at 4.7 T. *NMR in Biomedicine*, 21, 781–792. <https://doi.org/10.1002/nbm.1253>
- Lee, R. H., Couto e Silva, A., Lerner, F. M., Wilkins, C. S., Valido, S. E., Klein, D. D., & Lin, H. W. (2017). Interruption of perivascular sympathetic nerves of cerebral arteries offers neuroprotection against ischemia. *American Journal of Physiology - Heart and Circulatory Physiology*, 312(1), H182–H188. <https://doi.org/10.1152/ajpheart.00482.2016>
- Martin, A. J., Friston, K. J., Colebatch, J. G., & Frackowiak, R. S. J. (1991). Decreases in regional cerebral blood flow with normal aging. *Journal of Cerebral Blood Flow & Metabolism*, 11(4), 684–689. <https://doi.org/10.1038/jcbfm.1991.121>
- Otori, T., Katsumata, T., Muramatsu, H., Kashiwagi, F., Katayama, Y., & Terashi, A. (2003). Long-term measurement of cerebral blood flow and metabolism in a rat chronic hypoperfusion model. *Clinical and Experimental Pharmacology & Physiology*, 30(4), 266–272. <https://doi.org/10.1046/j.1440-1681.2003.03825.x>
- Powers, W. J. (1991). Cerebral hemodynamics in ischemic cerebrovascular disease. *Annals of Neurology*, 29(3), 231–240. <https://doi.org/10.1002/ana.410290302>
- Roloff, E. v. L., Tomiak-Baquero, A. M., Kasparov, S., & Paton, J. F. R. (2016). Parasympathetic innervation of vertebrobasilar arteries: Is this a potential clinical target? *Journal of Physiology*, 594(22), 6463–6485. <https://doi.org/10.1113/JP272450>
- Sercombe, R., Aubineau, P., Edvinsson, L., Mamo, H., Pinard, E., & Seylaz, J. (1975). Neurogenic influence on local cerebral blood flow. *Neurology*, 25, 954–963.
- Silesen, H., & Schroeder, T. (1989). Haemodynamic evaluation of carotid artery disease. *Clinical Physics and Physiological Measurement*, 10(Suppl A), 15–22. Retrieved from <https://www.ncbi.nlm.nih.gov/pubmed/2653704>
- Silva, D., & Belli, A. (2018). Critical care management of neurosurgical patients. In R. G. Ellebogen, L. N. Sekhar, & N. Kitchen (Eds.), *Principles of neurological surgery* (4th ed., p. 392). Philadelphia, PA: Elsevier. Retrieved from https://books.google.nl/books?id=GTdDDwAAQBAJ&pg=PA391&lpg=PA391&dq=physiological+stress+cpp+cbf&source=bl&ots=rvi7Hryofw&sig=ACfU3U0_NgvtoZOA01cK4z8ewk3_rBmTGg&hl=nl&sa=X&ved=2ahUKEwjx8baat7vgAhWELVAKHWGpCQMq6AEwChOECAIQAQ#v=onepage&q=physiological
- Tsuchiya, M., Sako, K., Yura, S., & Yonemasu, Y. (1992). Cerebral blood flow and histopathological changes following permanent bilateral carotid artery ligation in Wistar rats. *Experimental Brain Research*, 89(1), 87–92. <https://doi.org/10.1007/BF00229004>
- Tutino, V. M., Mandelbaum, M., Choi, H., Pope, L. C., Siddiqui, A., Kolega, J., & Meng, H. (2014). Aneurysmal remodeling in the circle of Willis after carotid occlusion in an experimental model. *Journal of Cerebral Blood Flow and Metabolism*, 34(3), 415–424. <https://doi.org/10.1038/jcbfm.2013.209>
- Ursino, M. (1994). Regulation of the circulation of the brain. In R. D. Bevan & J. A. Bevan (Eds.), *The human brain circulation: Functional changes in disease* (pp. 291–318). Totowa, NJ: Humana Press.
- Van Denderen, J. C. M., Van Wieringen, G. W., Hillen, B., & Bleys, R. L. A. W. (2001). Zinc sulphate-induced anosmia decreases the nerve fibre density in the anterior cerebral artery of the rat. *Autonomic Neuroscience: Basic & Clinical*, 94(1–2), 102–108. [https://doi.org/10.1016/S1566-0702\(01\)00354-X](https://doi.org/10.1016/S1566-0702(01)00354-X)

How to cite this article: Rots ML, de Borst GJ, van der Toorn A, et al. Effect of bilateral carotid occlusion on cerebral hemodynamics and perivascular innervation: An experimental rat model. *J Comp Neurol*. 2019;527:2263–2272. <https://doi.org/10.1002/cne.24672>